presence of handles is more significant when $d_V = 3$ compared to $d_V = 2$. The effect of a deflating pressure is to collapse the vesicle, thereby reducing d_V from 3 to 2. In this deflated regime, it does not pay to continue having the handles. The minimization of the volume accompanied by the divergence of the average surface area as one approaches the critical line favors the breaking up of handles into simpler topologies. In the restricted topology case, the handles are excluded or constrained. It is intriguing that this restriction plays a role similar to that of a deflating pressure leading to the collapsed limit. Our results suggest that even for a fluid membrane, in the absence of a pressure imbalance, the universality class may depend on whether there are restrictions on the number of handles or not.

Why should vesicles with unrestricted handles be fatter ($d_V = 3$) than those with restrictions? A possible mechanism for gaining entropy compared to the tubular configuration of Fig. 2 could be to have a proliferation of fat donut-like handles with very small holes (the baker's nightmare), the small holes can then be placed in many locations leading to a large entropy.

The difference between surfaces with restricted and unrestricted handles is further underscored by the fact that in the absence of self-avoidance and any interaction, the former remains well defined whereas the latter is characterized by an entropy that is not extensive (*16*) and is therefore ill-defined as a statistical mechanics model. The self-avoidance interaction is usually irrelevant above the upper critical dimension. In the case of unrestricted handles, this probably is not the case since the model needs a regulator to be well defined.

REFERENCES AND NOTES

1. See, for example, D. R. Nelson, in *Statistical Mechanics of Membranes and Interfaces*, D. R. Nelson, T. Piran, S. Weinberg, Eds. (World Scientific, Singapore, 1989); F. F. Abraham and D. R. Nelson, *Science* **249**, 393 (1990).
2. A. M. Polyakov, *Gauge Fields and Strings* (Harwood Academic, New York, 1982).
3. A self-avoiding, closed surface in three dimensions is orientable, see, for example, H. S. M. Coxeter, *Regular Complex Polytopes* (Cambridge Univ. Press, New York, 1974); *Introduction to Geometry* (Wiley, New York, 1969).
4. U. Glaus and T. L. Einstein, New York, *J. Phys.* **A20**, L105 (1987); U. Glaus, *J. Stat. Phys.* 50, 1141 (1988).
5. J. O'Connell *et al.*, in preparation.
6. G. Parisi and N. Sourlas, *Phys. Rev. Lett.* **56**, 871 (1981).
7. B. Durhuus, T. Jonsson, J. Frohlich, *Nucl. Phys.* **B240**, 453 (1984)
8. P. G. de Gennes, *Scaling Concepts in Polymer Physics* (Cornell Univ. Press, Ithaca, 1979).
9. A. Maritan and A. L. Stella, *Nucl. Phys.* **B280**, 561 (1982).
10. F. J. Wegner, *J. Math. Phys.* **12**, 2259 (1971).
11. L. P. Kadanoff, *Rev. Mod. Phys.* **59**, 267 (1977).
12. J. R. Banavar, A. Maritan, A. L. Stella, *Phys. Rev. A*, in press.
13. S. Leibler *et al., Phys. Rev. Lett.* **59**, 1989 (1987); M. E. Fisher, *Physica* **38D**, 112 (1989); C. J. Camacho and M. E. Fisher, *Phys. Rev. Lett.* **65**, 9 (1990).
14. A. Maritan and A. L. Stella, *Phys. Rev. Lett.* **53**, 123 (1984).
15. P. Pfeifer, U. Welz, H. Wippermann, *Chem. Phys. Lett.* **113**, 535 (1985).
16. T. Eguchi and H. Kawai, *Phys. Lett.* **110B**, 143 (1982).

17. We are grateful to M. Fisher and B. Harris for stimulating discussions and many helpful suggestions. We are indebted to J. Maynard for drawing the figures for us with DataScript Scientific Software. The work at Penn State was supported by grants from the NSF, NASA, and the Petroleum Research Fund administered by the American Chemical Society.

18 December 1990; accepted 13 March 1991

Ultradeep (>300 Kilometers) Ultramafic Xenoliths: Petrological Evidence from the Transition Zone

VIOLAINE SAUTTER, STEPHEN E. HAGGERTY, STEPHEN FIELD

The seismologically delineated transition zone, at depths between 400 and 670 kilometers, is a fundamental discontinuity in the earth that separates the upper mantle from the lower mantle. Xenoliths from within or close to the transition zone are dominated by pyropic garnet and associated pyroxene or mineralogically heterogeneous garnet lherzolite. These xenoliths show evidence for the high-pressure (90 to 120 kilobars) transformation of pyroxene to a solid solution of pyroxene in garnet (majorite) and silicon in octahedral coordination; low-pressure (less than 80 kilobars) exsolution of clinopyroxene or orthopyroxene from the original majorite is preserved. Although mineral modes and rock proportions below the transition zone and the relative amount of eclogite present cannot be accurately assessed from the xenoliths, it is likely that both majorite and β-spinel help produce the observed seismic gradient of the transition zone.

WHETHER THE DISCONTINUITY AT a depth of 400 km reflects an isochemical phase change from olivine to β-spinel (model 1) or a chemical change related to pyroxene dissolution in garnet (model 2) is controversial; a related issue is whether the mantle is homogeneous (*1*) or is stratified as a result of the transformation of peridotite at a depth of 400 km into piclogite [olivine eclogite (*2, 3*), model 2]. Because of the lack of natural samples, mineral assemblages and the mantle composition between depths of 200 km and the transition zone at 400 to 670 km have previously been indirectly inferred either from comparisons of elastic moduli of silicates and oxides with predictions from seismic velocity data or from results of high-pressure experimental investigations (*4–7*). Recently, however, deep mantle xenoliths have been identified from the vicinity of this discontinuity (*8*). These rocks were transported to the crust by an eruptive kimberlite at Jagersfontein, located close to the southeast edge of the Kaapvaal craton in South Africa. In this report we describe two additional samples from this pipe that help to characterize the relation between pyroxene and garnet and the compositional variation of this part of the mantle.

The mantle xenoliths that we described earlier from this kimberlite contain a close association of ultramafic pyrope-rich garnet [69 to 73% pyrope (on a mole basis), 15 to 20% almandine, and 11 to 12% grossular] substituted by Cr (up to 2% by weight Cr_2O_3) and ternary clinopyroxene (20% jadeite, 74% diopside, and 6% enstatite). The clinopyroxene forms either oriented <111> rods in the garnet host or is present as discrete crystals attached to garnet in a cuspate and sealed grain-boundary contact. Both textural types of pyroxene exsolved from garnet as a result of pressure release at a depth of 100 to 150 km from the original depth of 300 to 400 km. When the clinopyroxene component is recombined with the host garnets' composition, a garnet with excess Si is produced; the Si/Al atomic ratio of these garnets is similar to that of garnets in diamond inclusions from the Jagersfontein (*9*) and Monastary (*10*) diamond mines in South Africa and Sao Luiz in Brazil (*11*). This excess Si is in octahedral coordination (Si^{VI}), is associated with an Al^{VI} deficit (unbalanced by Cr and Ti), and is typical of the chemical signature of a pyroxene component dissolved in the garnet structure (*12*).

We have processed 324 samples (mostly in the range 0.5 to 3 cm in diameter) from Jagersfontein, of which about 10% contain

---

V. Sautter, Laboratoire de Géophysique et de Géodynamique Interne, Université de Paris–Sud, 91405 Orsay CEDEX, France.

S. E. Haggerty, Department of Geology, University of Massachusetts, Amherst, MA 01003.

S. Field, Department of Geology, Stockton State College, Pomona, NJ 08240.

garnets with exsolved pyroxene. Two different types of garnets containing exsolved pyroxene are recognized in the samples. One of these specimens (sample K7-318) is a four-phase garnet lherzolite (garnet, olivine, orthopyroxene, clinopyroxene); the second type consists of discrete crystals of garnet (sample JX90-1). Garnets in the lherzolite contain exsolved clinopyroxene (Fig. 1, A and B), whereas the discrete garnet specimen has exsolved orthopyroxene (Fig. 1C); these are designated, respectively, as group 1 and group 2. Samples from our earlier study (*8*) have ultramafic garnets and pyroxenes of eclogitic affinity (*13*). These samples fall into group 1 and are interpreted as probable fragments of lherzolites of unusual composition.

The garnet lherzolite (sample K7-318) is 9 by 6 cm, is coarse-grained with an average crystal size of 5 mm, and is heterogeneous in mineral proportions on a macro, and microscopic scale. Most of the sample is composed of 40 to 50% olivine, 30 to 40% orthopyroxene, and 5 to 10% clinopyroxene by volume: the texture is equigranular. A coarse-grained (5 to 10 mm) garnet-rich (70 to 80% by volume) band, 1 to 1.5 cm wide at one end of the xenolith, is intergrown with orthopyroxene (10 to 15% by volume) and minor olivine; the crystals have an irregular shape and curvilinear grain-boundary contacts. Garnets are a clear brilliant purple, the clinopyroxene is apple green, the orthopyroxene is bronze, and the olivine is glassy with minor serpentinization. The xenolith is permeated by decompression microfractures. In common with the garnets from our earlier study, the lherzolitic garnets are crowded with rod-shaped clinopyroxene lamellae along the <111> garnet directions (Fig. 1A), 100 to 200 μm long and <5 μm to a maximum of 50 μm wide; coarse (100 to 200 μm), equant, and subhedral platelets of clinopyroxene, however, are also present in sample K7-318 (Fig. 1B). Because of the contrasts in exsolution textures and uncertainty about the amount of grain-boundary pyroxene that may also represent exsolution from garnet-pyroxene solid solution, a conservative estimate for the majorite component is about 20% by volume. Mineral compositions of the dominant phase assemblage and of clinopyroxene exsolution in garnet (Table 1) show that olivine (92% forsterite) and orthopyroxene (90.1% enstatite, 7.4% ferrosilite, and 2.5% wollastonite) are typical of lherzolites. Garnet has 70 mole percent pyrope component and moderate Cr_2O_3, and the clinopyroxenes are solid solutions of diopside, enstatite, and jadeite.

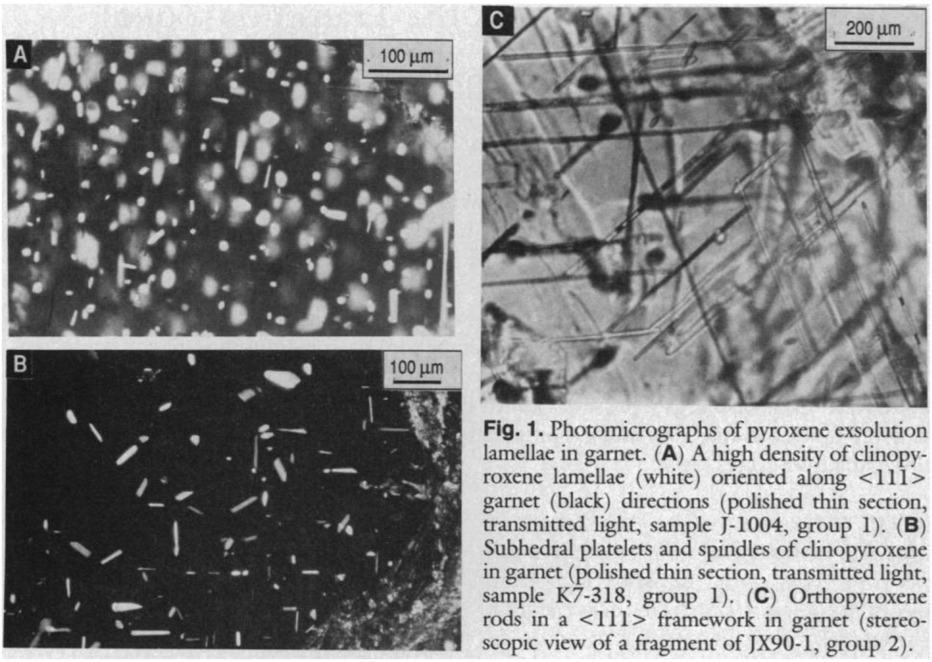

Fig. 1. Photomicrographs of pyroxene exsolution lamellae in garnet. (**A**) A high density of clinopyroxene lamellae (white) oriented along <111> garnet (black) directions (polished thin section, transmitted light, sample J-1004, group 1). (**B**) Subhedral platelets and spindles of clinopyroxene in garnet (polished thin section, transmitted light, sample K7-318, group 1). (**C**) Orthopyroxene rods in a <111> framework in garnet (stereoscopic view of a fragment of JX90-1, group 2).

Table 1. Results of electron microbeam chemical analyses of representative minerals in garnet lherzolite (sample K7-318). Values in oxide percent by weight are given in the upper part of the table; cations on the basis of 12 O atoms for garnet (Gt), 4 for olivine (Ol), and 6 for clinopyroxene (Cpx) (D = discrete large crystals and L = lamellae) are given in the lower part. Opx, orthopyroxene.

Component	Gt	Ol	Opx	Cpx(D)	Cpx(L)
SiO_2	42.00	40.96	56.90	54.18	54.15
TiO_2					
Al_2O_3	22.43		0.91	2.59	2.62
Cr_2O_3	2.19		0.36	1.02	1.68
FeO	8.95	8.25	5.15	1.69	2.01
MnO	0.41				
MgO	19.38	50.77	35.11	16.61	16.14
CaO	4.94		1.39	22.03	21.23
Na_2O			0.18	1.77	1.99
K_2O					
NiO		0.27			
Totals	100.30	100.25	100.00	99.89	99.82
Si	2.997	0.995	1.963	1.965	1.967
Ti					
Al	1.886		0.037	0.110	0.112
Cr	0.123		0.010	0.029	0.048
Fe	0.534	0.168	0.148	0.051	0.061
Mn	0.025				
Mg	2.061	1.839	1.806	0.898	0.874
Ca	0.378		0.051	0.856	0.826
Na			0.012	0.124	0.140
Ni		0.005			
Totals	8.004	3.007	4.027	4.033	4.028

Group 2 garnets are discrete pink garnet crystals (1 cm in diameter) with optically homogeneous orthopyroxene exsolution lamellae oriented along <111> directions in an open triangular network (Fig. 1C). The orthopyroxene lamellae vary from <5 to 20 μm wide; most lamellae are longer than 200 μm, some are discontinuous, but others span the entire garnet crystal. The proportion of orthopyroxene in the pink garnets does not exceed 15% by volume. Group 2 garnets are more pyrope-rich (up to 80 mole percent of the pyrope component) than group 1 garnets and are Cr-poor (less than 1% Cr_2O_3 by weight, Table 2). Orthopyroxene compositions are highly magnesian [$Mg/(Mg + Fe) = X_{Mg} = 0.95$], and contain minor Na, Cr, and Al (Table 2). The host rock to these garnets has yet to be identified but it is most likely ultramafic.

For reasons outlined in (*8*), we argued that the pyroxene rods in garnets were the products of exsolution from a homogeneous majorite solid solution. Exsolution that is induced by a disproportionation of a solid solution results in a rigorous orientation of the crystalline precipitate within the host. Precise interface relations are not necessarily produced in coprecipitation that may give rise to similar microscopic textures. Transmission electron microscopy observations on JX-50 from our earlier study indicate that the <001> direction in the pyroxene rods is parallel to the <111> direction in garnet. We had suggested that such a crystallographic relation would minimize Si and Al diffusion paths and thus facilitate the unmixing process (*14*). Pyroxene rods oriented parallel to the four <111> axes of the cubic garnet are surprisingly polycrystalline and have three different orientations of clinopyroxene around their <001> axes. This feature is related to the higher degree of symmetry in the cubic host relative to that in the exsolved monoclinic pyroxene structure. The relative orientation of the two phases is further described by (110) garnet parallel to (010) clinopyroxene. Pyroxene exsolution from garnet involves a major structural change and is a reconstructive process that proceeds by heterogeneous nucleation and growth. This thermally activated process is generally sluggish compared with displacive transformations (*15*).

The depth of origin of the lherzolite (sample K7-318), the group 1 assemblages from our earlier study (*8*), and the group 2 pink garnet macrocrysts (JX90-1) may be estimated if the exsolved pyroxene component is recombined back into the garnet. The reconstructed garnets are Al-deficient and contain excess Si. On the basis of the conservative volumetric estimates for the pyroxene component, the number of Si atoms on the basis of 12 O atoms is 3.2 for group 1 and 3.1 for group 2. The corresponding range for the unexsolved Ca-Na majorite inclusions in diamond is 3.1 to 3.4 Si atoms per 12 O atoms (*9–11*).

There have been several experimental calibrations for the transformation of pyroxene to garnet (*16*), but the system that is most comparable to our group 1 minerals and rock composition (lherzolite) is that used by Akaogi and Akimoto (*17*). For Si contents of 3.1 and 3.2 atoms per 12 O atoms and a temperature of 1200°C, pressures of 90 to 130 kbar, respectively, are estimated (Fig. 2). The extremely low Mg-Tschermak component that is associated with an abnormally high enstatite (95 mole percent) content in group 2 orthopyroxene exsolution lamellae implies, according to Akaogi and Akimoto (*17*), a pressure in excess of 70 kbar. Orthopyroxene dissolution in garnet in the Mg-Al-Si (MAS) system starts and is completed at lower pressures than clinopyroxene dissolution in garnet in the Ca-MAS system (*17*). Therefore, a more realistic pressure estimate for group 2 is 70 to 90 kbar. The transition of olivine to β-spinel modifies the Fe^{2+}-Mg^{2+} partitioning among the major minerals in lherzolites because β-spinel fractionates Fe (*17*). Consequently, adjacent pyroxenes and garnet reset their X_{Mg} ratio by increasing Mg over Fe. Experimentally, the onset of this change is 120 kbar. If the high X_{Mg} contents of the group 1 and group 2 assemblages are a reflection of β-spinel fractionation, then all of the garnet and exsolved clinopyroxene in ultramafic xenoliths from Jagersfontein could have come from a maximum depth of 400 km. Excess Si (>0.2) in garnet has been described both in Monastary and in Sao Luiz diamond inclusions (*10, 11*). For these eclogitic mafic compositions, the range of 3.2 to 3.4 Si atoms in garnet corresponds to a pressure range of 130 to 145 kbar (*18*), which is equivalent to a depth interval of 400 to 500 km. Even though the presence of Na may substantially expand the stability field of high-Si garnets to lower pressures (*16*), we consider that the starting material of mid-ocean ridge basalt of Irifune *et al.* (*18*) is probably a better analog for the garnet inclusions in diamond than the simplified enstatite-jadeite join (*16*). These comparisons substantiate that the pressures involved, and the depths inferred, correspond to those for rocks close to or within the transition zone. The reequilibration during decompression that drove the exsolution process in the xenoliths requires pressures below 80 kbar, which coincide with the onset of pyroxene dissolution in garnet. Temperatures estimated from the Fe-Mg and Ca-Mg partitioning between garnet and clinopyroxene and clinopyroxene and orthopyroxene, respectively, yield a range of 900° to 1000°C (*8*). Thus the rocks last equilibrated under relatively cool, low-pressure conditions that would correspond to the lithosphere.

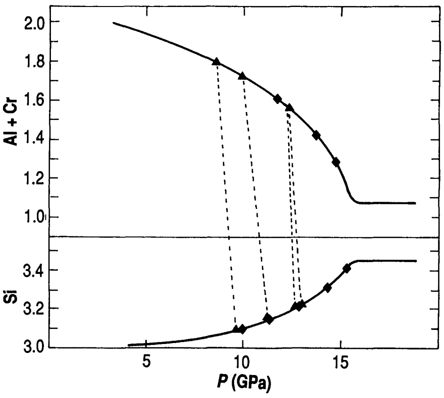

Fig. 2. Geobarometric estimates (*17, 18*) of reconstituted garnet and clinopyroxene (group 1) and garnet and orthopyroxene (group 2) assemblages (▲) based on excess Si (>3.0 Si atoms per 12 O atoms, Table 2) and Cr + Al. Homogeneous high-Si garnet inclusions in diamonds (*10*) are also shown (◆).

Table 2. Results of electron microbeam chemical analyses and reconstructed garnet (Gt), and clinopyroxene (Cpx) solid solutions for group 1, Gt:Cpx = 75:25; and group 2, Gt:Opx = 90:10 assemblages. Densities used in reconstitution calculation are given in (*8*). Opx, orthopyroxene. H = host garnet and L = lamellae of pyroxene. $M^* = Na + Ca + Mg + Mn + Fe^{2+}$.

Component	Group 1, sample JX-25			Group 2, sample JX-90-1		
	Gt(H)	Cpx(L)	Gt75Cpx25	Gt(H)	Opx(L)	Gt90Opx10
SiO_2	42.23	54.08	44.93	43.23	58.22	44.58
TiO_2	0.04	0.09	0.05	0.06	0.05	0.054
Al_2O_3	23.54	2.42	18.73	23.95	0.71	21.85
Cr_2O_3	1.53	1.20	1.45	1.02	0.14	0.94
FeO	7.70	1.76	6.35	5.67	3.27	5.45
MnO	0.48	0.02	0.37	0.24		0.22
MgO	20.38	15.40	19.24	22.55	37.02	23.85
CaO	4.56	22.39	8.625	4.04	0.17	3.69
Na_2O	0.06	2.33	0.58		0.01	
Totals	100.52	99.69	100.33	100.76	99.59	100.63
Si	2.979	1.970	3.193	2.999	1.984	3.090
Ti	0.002	0.002	0.003	0.003	0.001	0.003
Al	1.957	0.104	1.567	1.960	0.028	1.783
Cr	0.085	0.034	0.082	0.056	0.004	0.050
Fe	0.454	0.053	0.377	0.330	0.093	0.317
Mn	0.029		0.023	0.014		0.012
Mg	2.143	0.836	2.037	2.331	1.880	2.458
Ca	0.345	0.874	0.657	0.300	0.006	0.275
Na	0.008	0.165	0.079			0.002
Totals	8.002	4.038	8.018	7.993	3.996	7.990
M^*	2.972	1.928	3.113	2.975	1.980	3.063

From the xenolith and diamond inclusion data we infer that the mantle is a mixture of eclogite and lherzolite from ~400 to 670 km. Thus both the olivine to β-spinel transition and pyroxene dissolution in garnet account for the 400-km discontinuity. The seismic anomaly at 400 km is due mostly to the relatively fast transition from olivine to β-spinel (*19*) because transformations from pyroxene to garnet are comparatively slow and occur over much larger intervals at depth. The xenolith data do not at present permit evaluations of the degree of heterogeneity (centimeter to kilometer scale) in the mantle at these depths, but much heterogeneity is predicted if oceanic slabs pile up in the transition zone (*20, 21*). Kimberlites are thought to be associated with mantle plumes (*21*), perhaps originating in the lower mantle; therefore, xenoliths from, or with chemistries reflecting an origin deeper than, the transition zone should be anticipated.

REFERENCES AND NOTES

1. A. E. Ringwood, *Composition and Petrology of the Earth's Mantle* (McGraw-Hill, New York, 1975).
2. J. D. Bass and D. L. Anderson, *Geophys. Res. Lett.* **11**, 237 (1984).
3. D. L. Anderson and J. D. Bass, *Nature* **320**, 321 (1986).
4. F. I. Birch, *J. Geophys. Res.* **57**, 227 (1952).
5. D. L. Anderson, *Spec. Pap. Mineral. Soc. Am.* **3**, 85 (1970).
6. D. J. Weidner, in *Chemistry and Physics of Terrestrial Planets*, S. K. Saxena, Ed. (Springer-Verlag, New York, 1986), pp. 251–274.
7. T. S. Duffy and D. L. Anderson, *J. Geophys. Res.* **94**, 1895 (1989).
8. S. E. Haggerty and V. Sautter, *Science* **248**, 993 (1990).
9. H. Tsai, H. O. A. Meyer, J. Moreau, H. J. Milledge, in *Proceedings of the Second Kimberlite Conference*, F. R. Boyd and H. O. A. Meyer, Eds. (American Geophysical Union, Washington, DC, 1979), vol. 1, pp. 16–26.
10. R. O. Moore and J. J. Gurney, *Nature* **318**, 553 (1985).
11. M. C. Wilding, B. Harte, J. W. Harris, paper presented at the 28th International Geologic Congress, 9 to 19 July 1989, Washington, DC, vol. 3, pp. 359–360 (abstract).
12. M. Akaogi and S. Akimoto, *Phys. Earth Planet. Inter.* **15**, 90 (1977).
13. For mafic compositions, the Si content in garnet increases concomitantly with Na according to the coupled substitution: (*x*) $Na^{VIII}\ SI^{VI} = R^{2+}\ Al$. By contrast, for ultramafic compositions the number of Si atoms and M^{2+} (Ca, Mg, Mn, Fe^{2+}) increase in a complementary manner according to a second coupled substitution: (*y*) $(R^{2+}, Si)^{VI} = (Al, Al)^{VI}$. For compositions having both mafic and ultramafic affinities, coupling of these two substitutional schemes, (*x*) and (*y*), gives the following structural formulae: (*x*) + (*y*); $(Na_xR^{2+})\ (R^{2+}Si_{x+y}\text{-}R^{3+}{}_{2-2y-x})Si_3O_{12}$. Reconstructed garnets from group 1 having both affinities obey this complex structural formula. The compositional range of the Ca-Na majorite inclusions in diamonds from the Monastary mine (*10*) also corresponds to this double, coupled substitutional scheme.
14. This orientation would match the tetrahedral chains of Si in pyroxenes with the octahedral sites of garnet that contain both Si and Al under very high pressures (>80 kbar).
15. In a displacive transformation, the product phase results generally from shearing of the preexisting mineral without bond breaking as observed in reconstructive transformation. Displacive transformations are fast under a suitable driving stress and are almost independent of temperature (diffusionless).
16. T. Gasparik, *Contrib. Mineral. Petrol.* **103**, 389 (1989).
17. M. Akaogi and S. Akimoto, *Phys. Earth Planet. Inter.* **19**, 31 (1979).
18. T. Irifune, T. Sekine, A. E. Ringwood, W. O. Hibberson, *Earth Planet. Sci. Lett.* **77**, 245 (1987).
19. F. Guyot *et al.*, *Geophys. Res. Lett.* **18**, 89 (1991).
20. A. E. Ringwood, *J. Geol.* **90**, 611 (1982).
21. D. L. Anderson, *Theory of the Earth* (Blackwell Scientific, Oxford, 1989).
22. We thank the DeBeers Mining Company for access to Jagersfontein and logistical support. We acknowledge the comments by I. D. MacGregor and the anonymous reviewers. Supported under NSF grant EAR89-054046 (to S.E.H.) and the Centre National de la Recherche Scientifique for a grant from the INSU-DBT program, Theme 4: Fluids, minerals, and kinetics (to V.S.), contribution 252.

2 January 1991; accepted 5 March 1991

In Situ Biodegradation: Microbiological Patterns in a Contaminated Aquifer

EUGENE L. MADSEN, JAMES L. SINCLAIR,* WILLIAM C. GHIORSE

Conventional approaches for proving in situ biodegradation of organic pollutants in aquifers have severe limitations. In the approach described here, patterns in a comprehensive set of microbiological activity and distribution data were analyzed. Measurements were performed on sediment samples gathered at consistent depths in aquifer boreholes spanning a gradient of contaminant concentrations at a buried coal tar site. Microbial adaptation to polyaromatic hydrocarbons (PAHs) was demonstrated by mineralization of naphthalene and phenanthrene in samples from PAH-contaminated, but not adjacent pristine, zones. Furthermore, contaminant-stimulated in situ bacterial growth was indicated because enhanced numbers of protozoa and their bacterial prey were found exclusively in contaminated subsurface samples. The data suggest that many convergent lines of logically linked indirect evidence can effectively document in situ biodegradation of aquifer contaminants.

THE RELEASE OF ORGANIC CHEMICALS to waters and soils can have dire consequences for wildlife, ecosystem integrity, and water quality (*1*). Alleviation of environmental pollution by stimulating native microbiological populations to effect biodegradation processes is promising (*2*), but such "bioremediation technologies" are far from proven. Although indigenous microorganisms in samples from many natural settings have been shown to have the potential to effect pollutant elimination (*3, 4*), the extent to which biodegradation potential is expressed in situ usually is a matter for speculation. Proof of in situ biodegradation must show that the mass of pollutant compounds has decreased and that microorganisms are the causative agents. These two pieces of information are exceedingly difficult to obtain in a field setting because mass balances may be precluded by the open complexity of the site and because other abiotic attenuating processes (dilution, migration, volatilization, sorption) may occur simultaneously with biodegradation (*5*). In situ biodegradation has been documented successfully in field studies of ponds and soil plots (*6*), in which specific responses of microorganisms were distinguished from abiotic responses. In contrast, such studies have not been possible in ground-water aquifers because their inaccessibility and variability prevent implementation of replicated, statistically valid experimental designs. Thus, studies that directly and unequivocally demonstrate in situ biodegradation in aquifers are rare (*7*).

The majority of attempts to document in situ biodegradation in aquifers have used indirect observations. Typically an imperfect mass balance, based on computer modeling, is cited to show loss of a pollutant in water pumped from the aquifer (*8*); but this approach does not distinguish unambiguously between biotic and abiotic processes. Chemical data from ground-water or sediment samples also may suggest that putative biodegradation activity is accompanied by changes in reactants (for example, oxygen and nutrients) and products (for example, CO_2 or intermediary metabolites) which are indicative of known microbiological processes (*2, 9*). The case is strengthened if high numbers of microorganisms, especially of pollutant-degrading bacteria are found (*2, 10*). Further support may be garnered from laboratory biotransformation assays indicating that the pollutant is chemically modified or converted completely to CO_2 in samples from the site (*2, 4, 11*). However, no established combination of these measures is robust enough to constitute absolute proof of in situ biodegradation in aquifer sediments. Methodological improvements are needed. We used patterns of microbiological activity

---

Section of Microbiology, Division of Biological Sciences, Cornell University, Ithaca, NY 14853.

*Present address: NSI Technology Services, R. S. Kerr Laboratory, P.O. Box 1198, Ada, OK 74820.